

Quantitative probe of the dynamics of mass transfer of water in organic porous materials by means of neutron spectroscopy: The case of covalent triazine-based frameworks

Mohamed Zbiri^{1*}, Catherine M. Aitchison², Reiner S. Sprick², Andrew I. Cooper², Anne A. Y. Guilbert^{3#}

¹Institut Laue-Langevin, 71 Avenue des Martyrs, Grenoble Cedex 9 38042, France

²Department of Chemistry and Materials Innovation Factory, University of Liverpool, Crown Street, Liverpool L69 7ZD, U.K.

³Department of Physics and Centre for Plastic Electronics, Imperial College London, Prince Consort Road, London SW7 2AZ, U.K.

*zbiri@ill.fr

#a.guilbert09@imperial.ac.uk

We study the mass transfer and interaction of water through/two porous covalent triazine-based frameworks (CTFs), by neutron incoherent spectroscopy. Inelastic neutron scattering evidences an interaction between CTF-CN and water, not observed for CTF-2, and that is correlated with the large amount of bound water or very slow diffusing water observed for CTF-CN using quasi-elastic neutron scattering (QENS). The water dynamics is also impacted by CTF-2 but to a lesser extent. The translational diffusion of constrained water in CTF-2 is well quantified by fitting the QENS spectra.

Hydrogen has been suggested as the energy carrier of the future as it can be stored and does not emit greenhouse gases at the point of use. [1] However, most hydrogen is still produced using steam reforming processes emitting large amounts of carbon dioxide when produced. The generation of hydrogen using clean methods have therefore become an area of intense research. Photocatalytic water splitting has been of particular interest as it uses water and solar light, which are abundant on Earth surface. [2–5]

In the process, a catalyst is used to generate charge-carriers that facilitate water reduction and oxidation. The catalysts are typically inorganic semiconductors. [2,3] Tremendous progress has been made in recent years in terms of improving the catalyst materials and the overall systems. [1,6] Nevertheless, organic materials have received significant attention over the last decade as they can be synthesised using many potential building blocks, hence, allowing tuning of the materials properties. [4,7]

Particularly, carbon nitrides have been studied as organic photocatalysts. Carbon nitrides are usually made through high-temperature condensation reactions and, exhibit, as a result, many defects including end-groups. [8,9]

Therefore, unbranched conjugated polymers, [10–16] conjugated microporous polymers (CMPs), [17–24] covalent triazine-based frameworks (CTFs) [25–28] and covalent organic frameworks [29–33] have been extensively studied in recent years allowing for fine tuning of material properties. Several factors have been identified to be important for the activity of polymer photocatalysts, such as the ability of a photocatalyst to absorb light, [13,21,23] the position of the redox potentials, [13] exciton separation, [14] crystallinity, [29] and wetting of the surface. [15,17,20] In particular, wetting of the surface seems to be crucial for organic polymer photocatalysts. Commonly, large aromatic building blocks are used that have an adverse impact on wetting of the surface and, at the molecular level, on the interaction with water.

In the case of porous photocatalysts, such as COFs and CMPs, high Brunauer-Emmett-Teller surface areas (S_{ABET}) have been suggested to be partly responsible for their enhanced photocatalytic activity as active sites within the material can potentially be accessed by water. [18,29,34,35] However, water penetration into the network depends on the material polarity [29,34] and, the water dynamics have to be considered as it will greatly impact reaction kinetics. Previously it has been observed that the interaction of a photocatalyst with water is highly dependent on the structure as shown for non-porous unbranched polymer photocatalysts. [36,37] Measurements, such as water uptake do not provide any information about water dynamics and crucially, no information about interaction of water with the surface of the materials at the molecular level can be obtained.

Neutron incoherent spectroscopy is a useful technique to understand the dynamics and interaction of guest molecules in host materials. In particular, quasi-elastic neutron scattering (QENS) has been used to study diffusion pathways and relaxation timescales of lithium ions in inorganic battery active materials, [38] methane diffusion in metal organic frameworks, [39] and the rotational dynamics of hydrogen adsorbed in covalent organic frameworks. [40] QENS has also been used to study the state of water when interacting with oligonucleotide crystals [41] and porous organic cages [42] showing distinct differences between bulk water and confined water interacting with the crystal surface. We previously studied water penetration and dynamics for a polar dibenzo[*b,d*]thiophene sulfone and a fluorene CMP using QENS in the context of photocatalysis, [34] however, the materials in the study were vastly different in terms of their polarities and water uptake.

Here, we study the influence of the network structure on the dynamics of water transfer within the networks of CTFs by means of neutron incoherent spectroscopy (QENS and inelastic neutron scattering – INS). QENS enables us to study the underlying dynamics of water within the networks and INS allows us to draw conclusions about interactions of water with the network at the molecular level. We select as a model system the previously reported CTF-2, [25] which contains an apolar biphenyl-linker, and CTF-CN, [26] which contains a polar cyano-group in the linker, allowing us to study two structurally related porous materials that differ in the polarity of their struts.

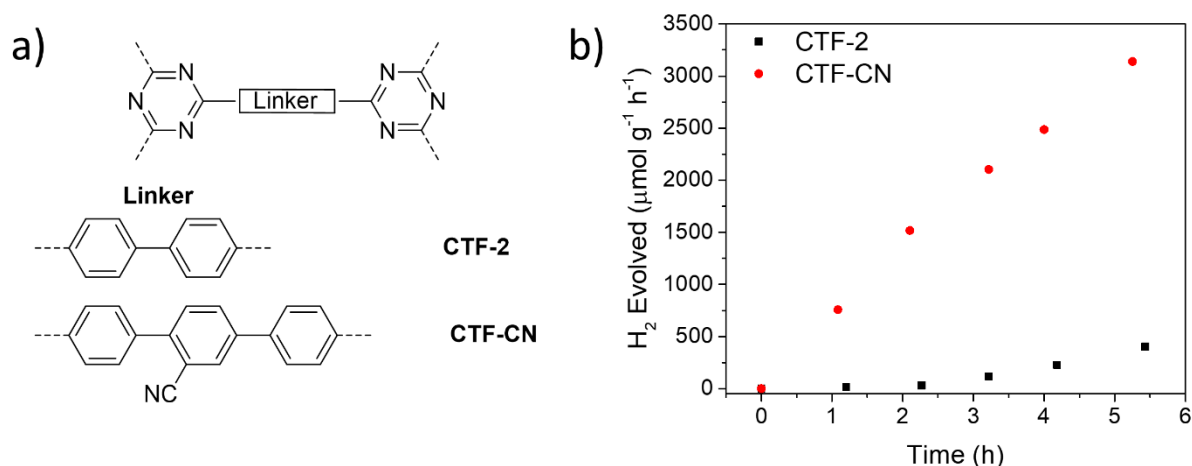


Figure 1. (a) Chemical structures of CTF2 and CTF-CN. (b) Hydrogen evolution of CTF-2 and CTF-CN. Linear hydrogen evolution rates were determined to be $118 \mu\text{mol h}^{-1} \text{g}^{-1}$ for CTF-2 and $595 \mu\text{mol h}^{-1} \text{g}^{-1}$ for CTF-CN. Conditions: Photocatalyst (25 mg loaded with 3 wt. % Pt by photodeposition of H_2PtCl_6) suspended in water/TEA (95:5 vol. %, 25 mL) illuminated by a 300 W Xe light source fitted with a $\lambda > 420 \text{ nm}$ filter.

Both CTF-2 [25] and CTF-CN [26] (Figure 1) were made using previously reported methods and tested as photocatalysts for hydrogen production from water in the presence of triethylamine. Platinum was added as a co-catalyst *via* photodeposition from H_2PtCl_6 and linear rates of $118 \mu\text{mol h}^{-1} \text{g}^{-1}$ for CTF-2 and $595 \mu\text{mol h}^{-1} \text{g}^{-1}$ for CTF-CN were determined (Figure 1b). Both materials were found to be porous to nitrogen with S_{ABET} determined to be $S_{\text{ABET}} = 873 \text{ m}^2 \text{g}^{-1}$ for CTF-2 and $548 \text{ m}^2 \text{g}^{-1}$ for CTF-CN (Figure 2a). The relatively high S_{ABET} of both materials together with the hydrophilic triazine building block in the materials may allow for water penetration into the network. From water sorption measurements (Figure 2b), CTF-2 shows a higher water uptake than CTF-CN possibly linked with the higher surface area of CTF-2 although condensation due to the interaction of water with the surface cannot be ruled out.

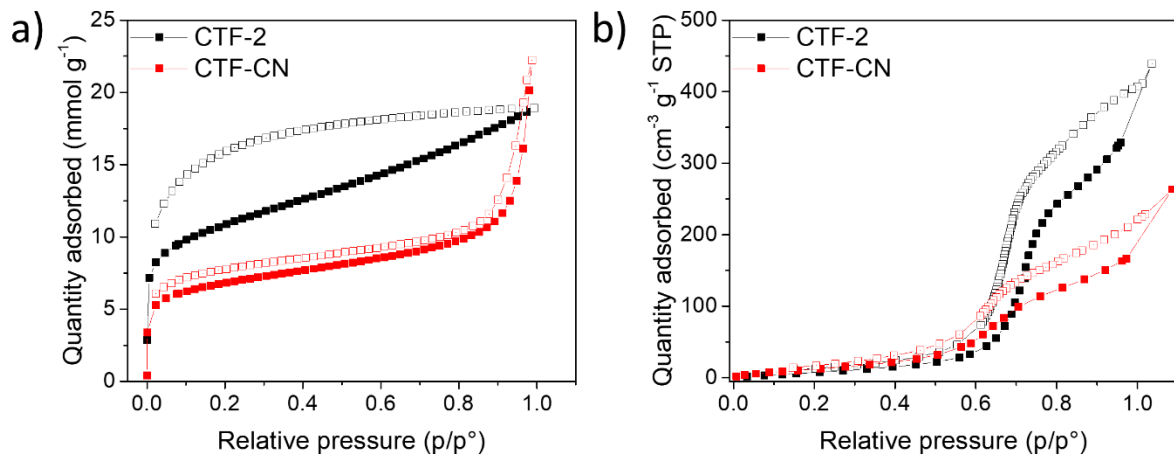


Figure 2. (a) Nitrogen sorption isotherm for CTF-2 and CTF-CN measured at 77.3 K and up to 1 bar (desorption curves shown as open symbols). (b) Water uptake isotherms for CTF-2 and CTF-CN measured at 293.15 K and up to 23.393 mbar (desorption curves shown as open symbols).

We went on to probe the molecular diffusivity of water at the surface/within the pores of the CTFs to quantify the internal mass transfer of water in this system using quasi-elastic neutron scattering (QENS). The QENS study is underpinned by an inelastic neutron scattering (INS) study to gain some further insights into the CTF-water (guest/host) dynamics. Neutron incoherent spectroscopy is very sensitive to hydrogens (see Table 1) and thus, is a method of choice for this study. Using deuterated water (D_2O) enables us to further tune the contrast between the CTFs and water and reveals the impact of water on the CTFs molecular motions.

Table 1. Neutron incoherent cross section in cm^{-1} of the samples studied in this work. The density of the CTFs is taken to be 0.8 g cm^{-3} .

| Water concentration (wt. %) | CTF-CN | CTF-2 | H_2O | D_2O |
|--------------------------------|--------|-------|----------------------|----------------------|
| 0.0 | 1.707 | 1.933 | | |
| 100.0 | | | 5.621 | 0.138 |
| 21.0 | 0.358 | | 4.441 | |
| 20.6 | 0.352 | | | 0.110 |
| 33.3 | | 0.644 | 3.749 | |
| 35.7 | | 0.690 | | 0.089 |

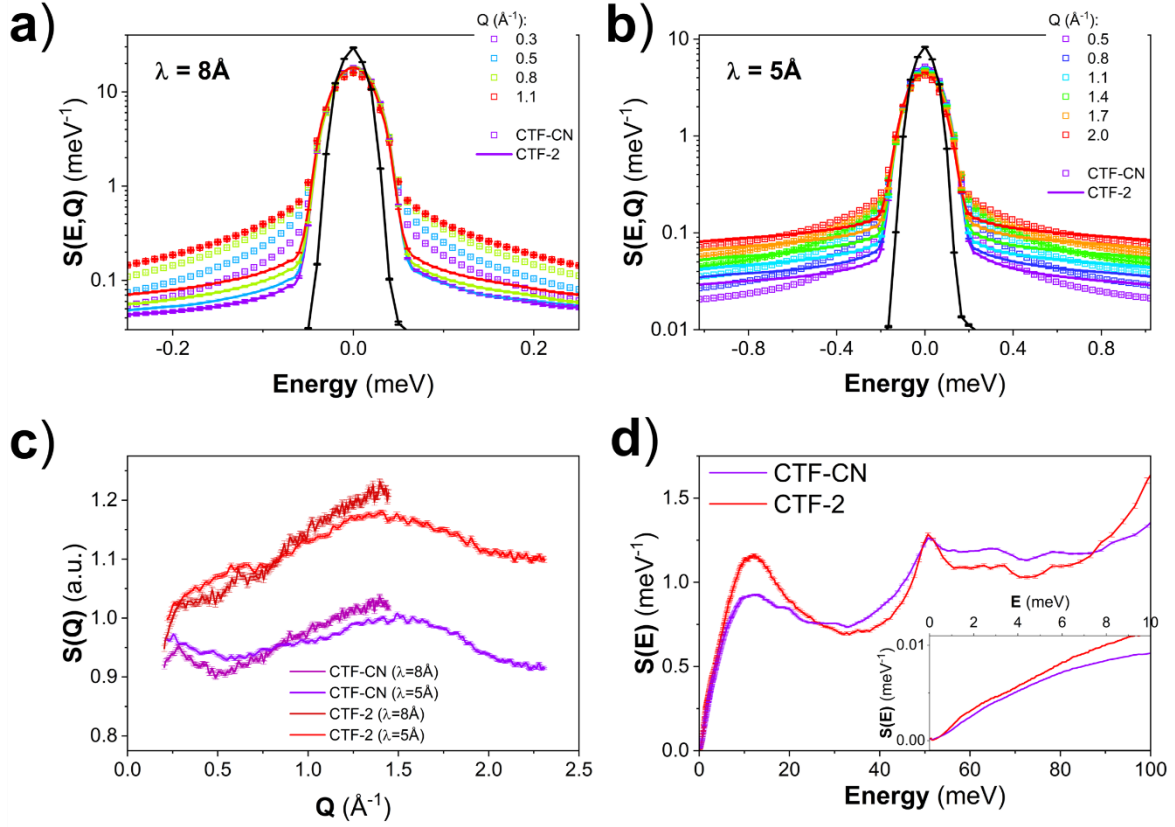


Figure 3. (a-b) Q -dependent QENS spectra of dried CTF-CN and CTF-2 using two neutron incident wavelengths (two different instrumental resolutions) (a) $\lambda = 8 \text{ \AA}$ and (b) $\lambda = 5 \text{ \AA}$. The instrumental resolution function from a vanadium sample is shown as the narrow black solid elastic line. (c) Neutron diffractograms of CTF-CN and CTF-2 extracted from the measurements using the two wavelengths. (d) Generalized phonon density of states (GDOS) [43] of CTF-CN and CTF-2 using $\lambda = 5 \text{ \AA}$. The inset shows the evolution of the Debye growth in the 0-10 meV region.

Figure 3 presents the QENS signals of the dried CTF-CN and CTF-2 using two neutron incident wavelengths, 5 \AA and 8 \AA . From the same measurements, we also extracted the respective neutron diffractograms and generalised phonon density of states (GDOS). [43] In line with their powder X-ray diffraction patterns, [25,26] both CTFs appear rather amorphous with a broad diffraction peak at around 1.5 \AA^{-1} (Figure 3 c). The Q -range from the 8 \AA setting is obviously reduced compared to 5 \AA . CTF-CN seems to exhibit another Bragg peak at low Q s, $\sim 0.3 \text{ \AA}^{-1}$. Although the QENS signal features some resemblance with a strong elastic contribution, CTF-CN exhibits noticeable dynamics within the covered energy range, either at 5 \AA and 8 \AA . CTF-CN has a longer linker with three benzene rings; thus, it can be expected that CTF-CN is softer than CTF-2 and hence, exhibits more pronounced dynamics. This is supported by the GDOS where similar features, phonon bands and the slope of the Debye growth, are observed for both CTFs. These features are more pronounced in the case of CTF-2, pointing towards a stiffer and more frustrated aspect of the structure of CTF-2. Moreover, the Debye growth of CTF2 seems slightly red-shifted with respect to that of CTF-CN, which points towards CTF-2 being more disordered than CTF-CN.

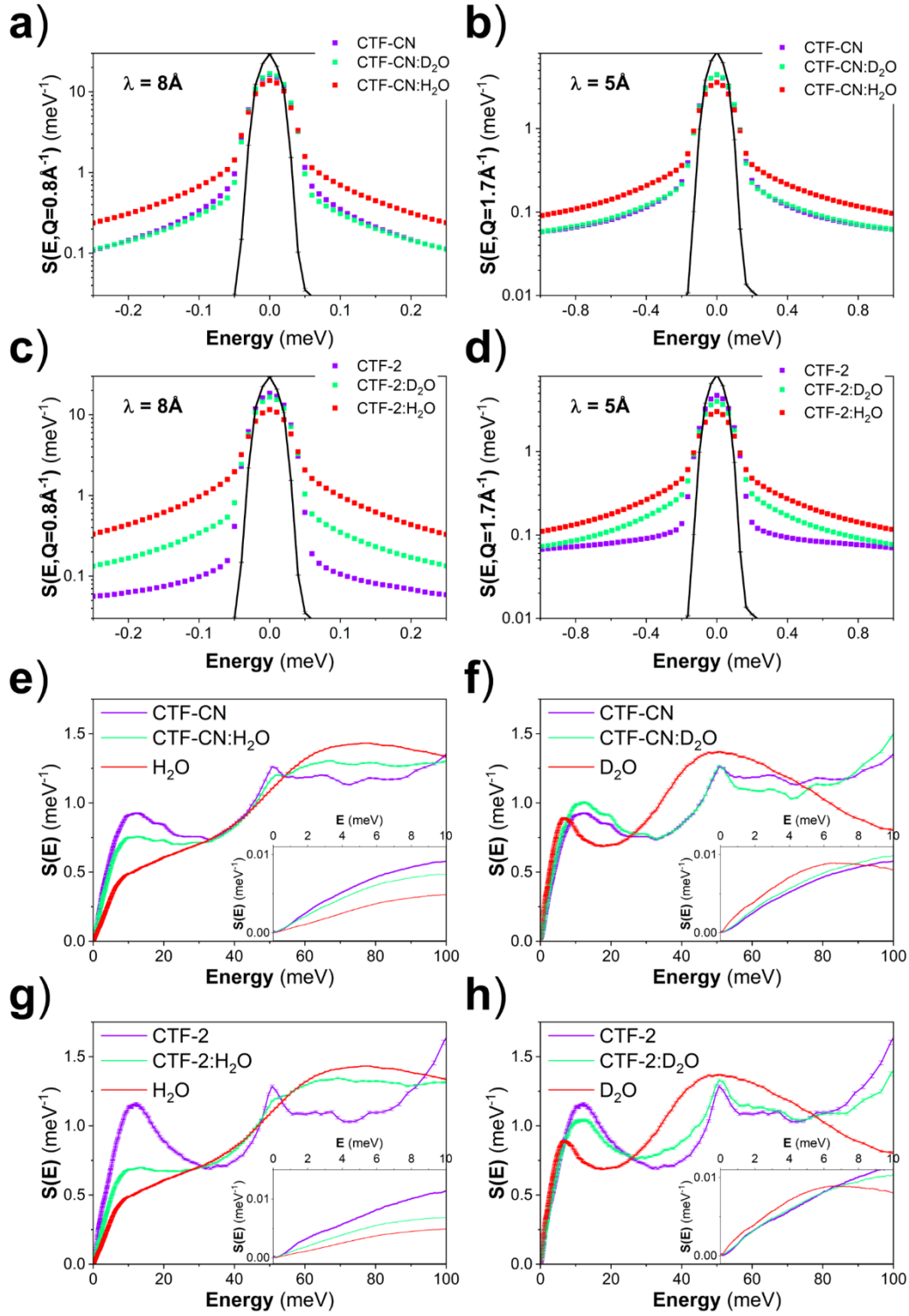


Figure 4. (a-d) QENS spectra of (a,b) CTF-CN and (c,d) CTF-2, dried, with H₂O and D₂O, using two neutron incident wavelengths (two different instrumental resolutions) (a,c) $\lambda = 8 \text{ \AA}$ and (b,d) $\lambda = 5 \text{ \AA}$. The instrumental resolution function from a vanadium sample is shown as the narrow black solid elastic line. (e-h) Generalized phonon density of states (GDOS) of CTF-CN and CTF-2 using $\lambda = 5 \text{ \AA}$ of (e,f) CTF-CN, dried, with H₂O and D₂O and (g,h) CTF-2, dried, with H₂O and D₂O. The inset shows the evolution of the Debye growth in the 0-10 meV region.

Figure 4 shows the QENS and GDOS spectra of CTF-CN and CTF-2, both dried and mixed with either H₂O or D₂O. When D₂O is added, no noticeable differences, as compared to the dried case, are observed in the QENS spectra for CTF-CN while a broadening is observed in the case of CTF-2. In both cases, the expected contribution to the total QENS spectra from the CTF material is supposed to be larger than from D₂O although to a lesser extent for CTF-CN (Table 1), as stemming from the difference in the incoherent neutron cross-section. For CTF-CN, a slight narrowing of the QENS signal is observed at the highest incident wavelength (8 Å), indicating potentially a further frustration of the structure when water is present. Interestingly, almost no differences are observed in the GDOS of CTF-2 upon addition of D₂O while the changes in GDOS spectra of CTF-CN cannot be simply explained by a weighted average of the spectra of the CTF and D₂O, especially for the strength of the peak around 10 meV. Moreover, a red-shift in the Debye growth with respect with the dried sample is observed for CTF-CN but not for CTF-2. This points towards the occurrence of specific interactions between CTF-CN and water leading to a further softening of the structure, which can be probably assigned to the presence of the -CN group in CTF-CN providing a site for interaction with water. [26] When H₂O is added to the CTFs, in both cases, a strong broadening of the QENS signals is observed. The GDOS in that case are dominated by the H₂O signal and no clear indication of interactions can be seen without further analysis.

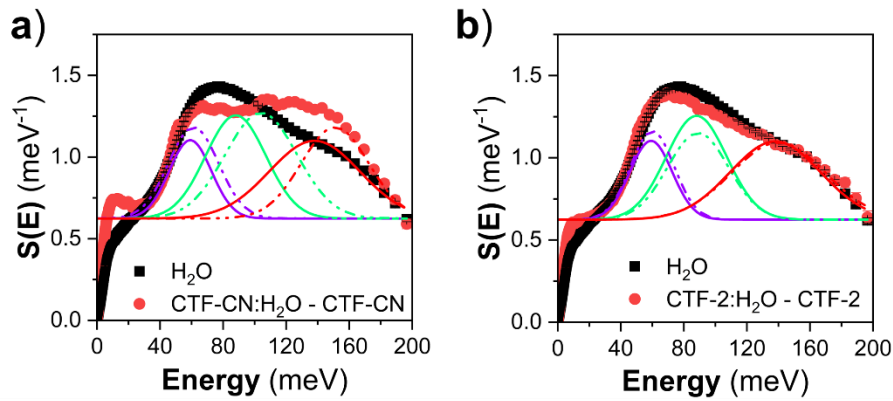


Figure 5. Generalised phonon density of states (GDOS) spectra of bulk reference H₂O and H₂O in (a) CTF-CN and (b) CTF-2, from measurements at 5 Å. The GDOS of H₂O in the CTF samples is presented here as the difference of the water-mixed CTFs (either CTF-CN:H₂O or CTF-2:H₂O) and dried CTFs (either CTF-CN or CTF-2, respectively). The broad peak at around 80 meV is assigned to the libration of water and is fitted with a combination of 3 Gaussians representing the rock, wag, and twist modes of water. [44,45]

Insights into the specific behaviour of water in the two CTFs can be gained by exploiting the GDOS of water and water-mixed CTFs. Figure 5 shows the GDOS of H₂O as a “reference”, compared to the difference of the GDOS of the water-mixed CTFs, CTF-2:H₂O or CTF-CN:H₂O, and dried CTFs, CTF-2 and CTF-CN, respectively. The comparison clearly highlights a pronounced hindrance and change in the vibrational distribution of the librational degrees-of-freedom of H₂O in CTF-CN as compared to H₂O in CTF-2. The intensity of the low-energy feature of water, at approximately 10 meV, increases for both CTFs although more significantly for CTF-CN. This could reflect a change in organisation of water, especially in the hydration monolayer of both CTFs, with a more pronounced effect in CTF-CN. The hindrance of the librational degrees-of-freedom of water in CTF-CN is a clear indication of the transition from free water to constrained/trapped water and/or bound water. This reflects a more favourable interaction of H₂O and CTF-CN, than for H₂O and CTF-2.

The QENS signals can be fitted to extract quantitative information about the mass transfer of water within the present CTF materials and also to estimate the amount of bound water in both CTFs. The dynamic structure factor of water $S_{\text{water}}(Q, \omega)$ can be expressed as a convolution of the dynamic structure factors of the vibrational $S_v(Q, \omega)$, translational $S_T(Q, \omega)$ and rotational motions of water $S_R(Q, \omega)$. [46]

$$S_{\text{water}}(Q, \omega) = S_v(Q, \omega) \otimes S_T(Q, \omega) \otimes S_R(Q, \omega)$$

$S_v(Q, \omega)$ can be written as: $S_v(Q, \omega) = A(Q)\delta(\omega) + B(Q)$. $A(Q)$ is proportional to the Debye-Waller factor, $\delta(\omega)$ is a Dirac function and $B(Q)$ is a background due to vibrations. $S_T(Q, \omega)$ can be represented by a single Lorentzian function $L(\omega, \Gamma_T(Q))$ of half width at half maximum (HWHM) $\Gamma_T(Q)$. $S_R(Q, \omega)$ is expressed following the well-known Sears formalism: [47,48]

$$S_R(Q, \omega) = j_0^2(Qa)\delta(\omega) + 3j_1^2(Qa)L\left(\omega, \frac{h}{3\tau_R}\right) + 5j_2^2(Qa)L\left(\omega, \frac{h}{\tau_R}\right)$$

where j_k is the k^{th} Bessel function, a is the radius of rotation and is taken to be the O-H distance in water molecule (0.98 Å), h is the reduced Planck constant and τ_R denotes the relaxation time of rotational diffusion. Considering the resolution of the instrument $R(\omega)$ and the above equations, the QENS signal of water $I_{\text{water}}(Q, \omega)$ can be rewritten as follow:

$$I_{\text{water}}(Q, \omega) = S_{\text{water}}(Q, \omega) \otimes R(\omega) = A(Q) \left\{ \left[j_0^2(Qa)L(\omega, \Gamma_T(Q)) + 3j_1^2(Qa)L\left(\omega, \Gamma_T(Q) + \frac{h}{3\tau_R}\right) + 5j_2^2(Qa)L\left(\omega, \Gamma_T(Q) + \frac{h}{\tau_R}\right) \right] \otimes R(\omega) \right\} + B(Q)$$

Within the random-jump-diffusion model, [49] the Q-dependence of Γ_T is given as follow:

$$\Gamma_T(Q) = \frac{D_T Q^2}{1 + D_T \tau_0 Q^2}$$

where D_T and τ_0 are the translational diffusion constant and the residence time of the translational diffusion, respectively. In the low-Q limit, $\Gamma_T(Q)$ can be approximated by $D_T Q^2$ while in the high-Q limit, $\Gamma_T(Q)$ is approximately equal to τ_0^{-1} .

Here, we use two wavelengths (5 Å and 8 Å) to enhance the resolution (8 Å) at low Q and to cover an extended Q-range (5 Å). Indeed, 5 Å gives a resolution of ~0.1 meV and a Q-range of 0.2-2.3 Å⁻¹ while 8 Å offers a resolution of 0.03 meV but a limited Q-range of 0.1-1.3 Å⁻¹. This should enable us to capture suitably both the translational and rotational motions of water.

We fit the QENS spectra of water using the above described model. $A(Q)$, $B(Q)$, $\Gamma_T(Q)$ and τ_R are fitted for both wavelengths, 5 Å and 8 Å, and for all the Qs. τ_R is shared through the entire dataset and $\Gamma_T(Q)$ are shared between the two wavelengths for the overlapping Q-range. The results of the fits are presented in Figure 6. The adopted model fits well both H₂O and D₂O. The Q-dependence of

the extracted HWHM for H₂O follows the expected model behaviour, and the extracted values for τ_R , D_T and τ_0 are in a good agreement with the literature (see Table 2). Although the same behaviour is observed for D₂O for Q-values up to 1.4 Å⁻¹, a different trend is observed for higher Qs, because D₂O presents a strong Bragg peak centred at higher Q, around ~ 1.8 Å⁻¹. Thus, the corresponding QENS spectra cannot be properly fitted and are therefore discarded.

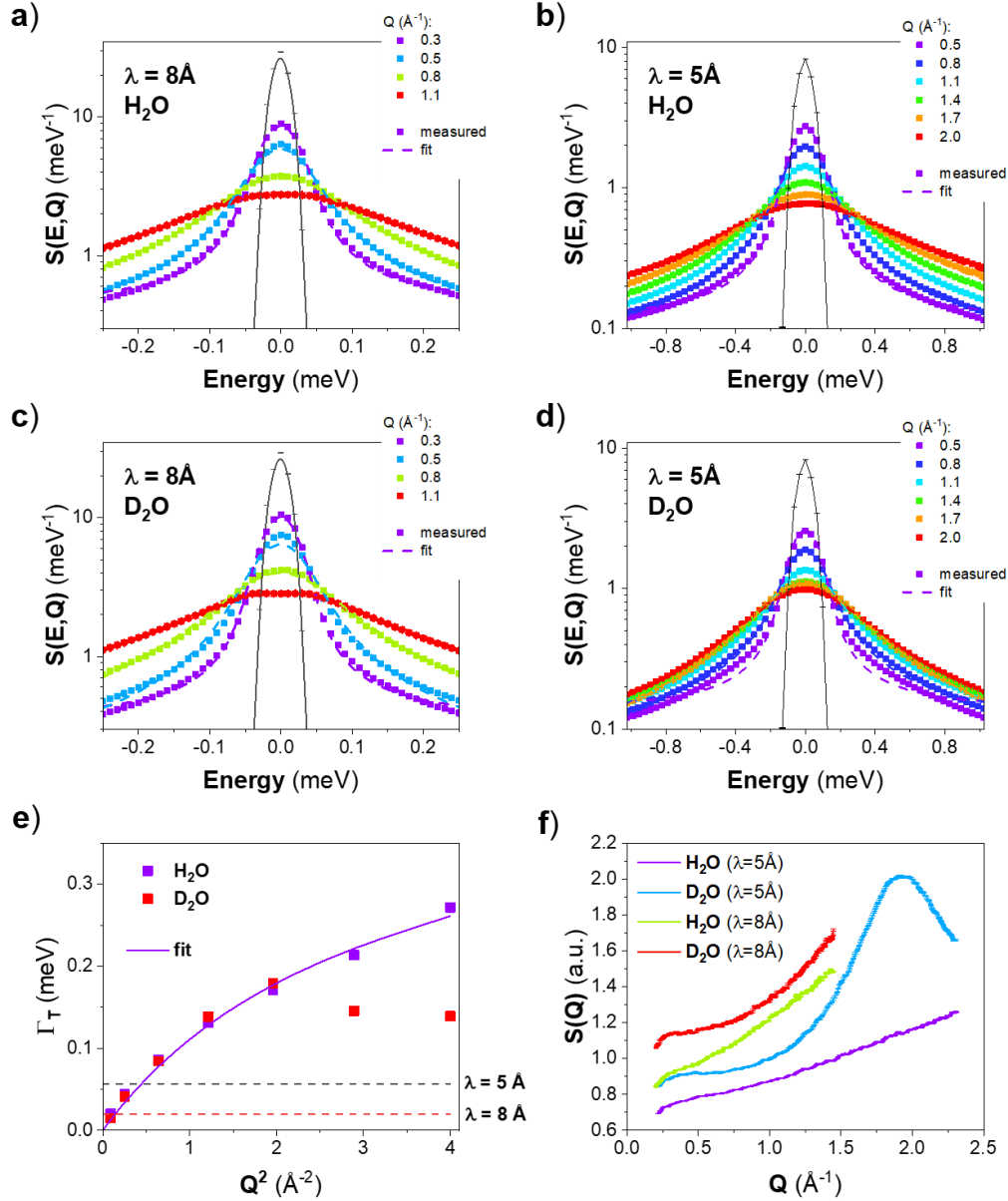


Figure 6. (a-d) QENS spectra, and their fit (dashed line), of H₂O (a-b) and D₂O (c-d) using two neutron incident wavelengths (two different instrumental resolutions) (a,c) $\lambda = 8 \text{ Å}$ and (b,d) $\lambda = 5 \text{ Å}$. (e) HWHM, extracted from the fit of QENS spectra of H₂O and D₂O, as a function of Q^2 , and the corresponding fit using the random-jump-diffusion model. The horizontal dashed lines represent the instrumental energy resolutions at $\lambda = 8 \text{ Å}$ and $\lambda = 5 \text{ Å}$. (f) Neutron Diffractograms of H₂O and D₂O extracted from the measurements using the two wavelengths.

We fit the QENS signals of the two CTF materials using the same model for water to account for both constrained and free water, and by adding an extra contribution for the CTF as follow:

$$I(Q, \omega) = (S_{CTF}(Q, \omega) + S_{water}(Q, \omega)) \otimes R(\omega)$$

$$= C \times I_{CTF}(Q, \omega) + (1 - C) \times A(Q) \times \left\{ \left[j_0^2(Qa) L(\omega, \Gamma_T) + 3j_1^2(Qa) L\left(\omega, \Gamma_T(Q) + \frac{h}{3\tau_R}\right) + 5j_2^2(Qa) L\left(\omega, \Gamma_T(Q) + \frac{h}{\tau_R}\right) \right] \otimes R(\omega) \right\} + B(Q)$$

where C is a shared parameter reflecting the concentration of water in the sample, weighted by the neutron incoherent cross-sections. Thus, it can, in principle, be calculated from Table 1. However, the presence of bound water can lead to an extra elastic contribution. The QENS signals of the CTFs exhibit a stronger elastic component than for bulk water and thus, the difference between C extracted from the fit and calculated from Table 1 can be used to derive an estimate of the amount of bound water. No significant differences in the neutron diffractograms of the CTFs are observed upon addition of water (see Supporting Information Figure S1) $A(Q)$ is fixed here and taken to be equal to the values extracted from the fit to the free water (see Supporting Information Table S1).

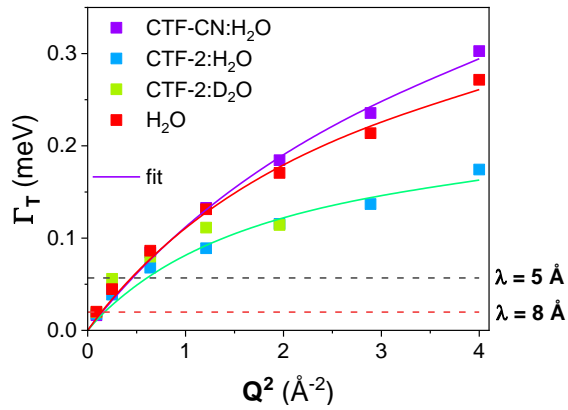


Figure 7. HWHM, extracted from the fit of the QENS spectra (see Supporting Information Figure S2), as a function of Q^2 , and the corresponding fit using the random-jump-diffusion model for CTF-CN:H₂O, CTF-2:H₂O and CTF-2:D₂O. The horizontal dashed lines represent the instrumental energy resolutions at $\lambda = 8$ Å and $\lambda = 5$ Å. The QENS spectra of CTF-CN:D₂O are not fitted as we observed no significant differences between the QENS spectra of CTF-CN and CTF-CN:D₂O (Figure 4 a,b).

Figure 7 presents the HWHM of the Lorentzian fits, of the QENS spectra, that accounts for the translational motion of water for the different samples presently studied, except CTF-CN:D₂O. No differences between free water and the water in CTF-CN is observed within the error of the experiment/fit while water in CTF-2 appears to be constrained with a slower translational diffusion and a longer residence time. We could fit the CTF-2:D₂O sample at lower Q s (the higher Q s being impacted by a strong Bragg peak of D₂O) and the extracted HWHM overlaps with the one extracted from the CTF-2:H₂O. It can be concluded from the very small change in the elastic peak between CTF-2 and CTF-2:D₂O (Figure 4 c-d) combined with the HWHM overlap that almost no differences in dynamics is observed on the covered energy range for CTF-2. The differences observed in Figure 4 c-d are mainly due to the presence of constrained D₂O and to the higher concentration of D₂O used than for CTF-CN. For both CTFs, about 10 wt. % of water (Table 2) is either subjected to too slow motions, not captured by the instrumental time window, or is bound to the CTFs. This amount is seemingly slightly higher in the case of CTF-CN, which would be consistent with the changes observed in the GDOS spectra.

Table 2. Main fitting parameters for H₂O and values from literature. [46] More parameters can be found in the Supporting Information (Table S1-2).

| | C | | Bound water | τ_R | D_T | τ_T | χ^2 |
|--|-----------------|-----------------|--------------------|----------------------------|---|----------------------------|----------------------------|
| | <i>expected</i> | <i>from fit</i> | (wt. %) | (ps) | (10 ⁻⁵ cm ² s ⁻¹) | (ps) | |
| from ref. [46] | | | | 1.10 | 2.3 | 1.10 | |
| H₂O | | | | 0.940 | 2.279 | 1.425 | 5.36 |
| CTF-CN:H₂O (21.0 wt. % H₂O) | 0.533 | 0.778 | 12.3 | 1.316 | 2.120 | 1.056 | 10.24 |
| CTF-2:H₂O (33.3 wt. % H₂O) | 0.408 | 0.531 | 9.4 | 1.296 | 1.958 | 2.752 | 15.59 |

To summarise, the GDOS reveals an interaction between CTF-CN and water, not observed in the case of CTF-2. This is inconsistent with the presence of the polar cyano-group in CTF-CN. QENS further reveals that the translational diffusion of water is slightly reduced in CTF-2 but it resembles bulk water for CTF-CN. A larger amount of bound water is estimated for CTF-CN. Note that (i) our model does not discriminate between bound water and water with motions too slow to be captured by the instrument and, that (ii) the diffusion coefficient estimated from our model is an effective average between the diffusion coefficient of constrained water and free water. Therefore, in light of the evidence of a stronger interaction between CTF-CN and water, and the larger amount of “bound” water extracted for CTF-CN, it is reasonable to conclude that water is more strongly affected by CTF-CN than CTF-2. The stronger interactions between water and CTF-CN is beneficial to the overall photocatalytic activity. However, it is not clear yet whether the observed difference in terms of dynamics stems from the first monolayer (hydration layer) or it is due to the constrained water within the pores and if the photocatalytic activity can be further improved by improving the water diffusion. Overall, the study evidenced a difference in the interaction between the CTFs and water, that have direct impact on the organisation and the guest-host dynamics of water in contact with the CTFs.

Experimental Details

The neutron scattering measurements were performed on the direct geometry, cold neutron, disc chopper time-of-flight spectrometer IN5 at the Institut Laue Langevin (Grenoble, France). An optimized sample thickness of 0.2 mm was considered, relevant to the minimization of effects like multiple scattering and absorption. Data were collected at 300K using two incident neutron wavelengths 5 Å ($E_i \approx 3.27$ meV) and 8 Å ($E_i \approx 1.28$ meV), offering an optimal energy resolution at the elastic line of ~ 0.1 and 0.03 meV, respectively. Standard corrections including detector efficiency calibration and background subtraction were performed. A vanadium sample was used to calibrate the detectors and to measure the instrumental resolution under the same operating conditions. At the wavelengths used, the IN5 angular detector coverage corresponds to a Q-range of $\sim 0.2\text{--}2.3$ Å⁻¹ ($\lambda_i = 5$ Å) and $\sim 0.1\text{--}1.3$ Å⁻¹ ($\lambda_i = 8$ Å). The data reduction and analysis were done using ILL software tools to extract the QENS spectra and the INS spectra in terms of the generalized density of states (GDOS). [43] For the QENS spectra, different data sets were extracted either by performing a full Q-average in the (Q, E) space to get the scattering function S(E, T) or by considering Q-slices to study the S(Q, E, T). The INS spectra were measured concomitantly with the acquisition of the QENS data, in the up-scattering, neutron energy-gain mode, and the one-phonon GDOS were extracted subsequently, within the incoherent approximation framework [50-52].

Acknowledgments

A.A.Y.G. acknowledges the Engineering and Physical Sciences Research Council (EPSRC) for the award of an EPSRC Postdoctoral Fellowship (EP/P00928X/1). C.M.A, A.I.C and R.S.S thank EPSRC for the financial support under Grant EP/N004884/1. Rob Clowes is thanked for help with the sorption measurements. The Institut Laue-Langevin (ILL) facility (Grenoble, France) is acknowledged for providing beam time on the IN5 spectrometer.

References

- [1] Y. Zhao, C. Ding, J. Zhu, W. Qin, X. Tao, F. Fan, and R. Li, *Angew. Chem. Int. Ed.* **2** (2020).
- [2] T. Takata and K. Domen, *ACS Energy Lett.* **4**, 542 (2019).
- [3] Z. Wang, C. Li, and K. Domen, *Chem. Soc. Rev.* **48**, 2109 (2019).
- [4] J. Jayakumar and H. Chou, *ChemCatChem* cctc. 201901725 (2020).
- [5] G. Zhang, Z.-A. Lan, and X. Wang, *Angew. Chemie Int. Ed.* **55**, 15712 (2016).
- [6] Q. Wang, T. Hisatomi, Q. Jia, H. Tokudome, M. Zhong, C. Wang, Z. Pan, T. Takata, M. Nakabayashi, N. Shibata, Y. Li, I. D. Sharp, A. Kudo, T. Yamada, and K. Domen, *Nat. Mater.* **15**, 611 (2016).
- [7] X. Wang, G. Zhang, and Z.-A. Lan, *Angew. Chemie, Int. Ed.* **55**, 15712 (2016).
- [8] X. Wang, K. Maeda, A. Thomas, K. Takanabe, G. Xin, J. M. Carlsson, K. Domen, and M. Antonietti, *Nat. Mater.* **8**, 76 (2009).
- [9] D. Kong, Y. Zheng, M. Kobielski, Y. Wang, Z. Bai, W. Macyk, X. Wang, and J. Tang, *Mater. Today* **21**, 897 (2018).
- [10] S. Yanagida, A. Kabumoto, K. Mizumoto, C. Pac, and K. Yoshino, *J. Chem. Soc. Chem. Commun.* 474 (1985).
- [11] S. Matsuoka, T. Kohzaki, A. Nakamura, C. Pac, and S. Yanagida, *J. Chem. Soc. Chem. Commun.* **39**, 580 (1991).
- [12] R. S. Sprick, B. Bonillo, R. Clowes, P. Guiglion, N. J. Brownbill, B. J. Slater, F. Blanc, M. A. Zwijnenburg, D. J. Adams, and A. I. Cooper, *Angew. Chemie Int. Ed.* **55**, 1792 (2016).
- [13] R. S. Sprick, C. M. Aitchison, E. Berardo, L. Turcani, L. Wilbraham, B. M. Alston, K. E. Jelfs, M. A. Zwijnenburg, and A. I. Cooper, *J. Mater. Chem. A* **6**, 11994 (2018).
- [14] J. Kosco, M. Bidwell, H. Cha, T. Martin, C. T. Howells, M. Sachs, D. H. Anjum, S. Gonzalez Lopez, L. Zou, A. Wadsworth, W. Zhang, L. Zhang, J. Tellam, R. Sougrat, F. Laquai, D. M. DeLongchamp, J. R. Durrant, and I. McCulloch, *Nat. Mater.* (2020).
- [15] R. S. Sprick, K. J. Cheetham, Y. Bai, J. Alves Fernandes, M. Barnes, J. W. Bradley, and A. I. Cooper, *J. Mater. Chem. A* (2020).
- [16] P.-J. J. Tseng, C.-L. L. Chang, Y.-H. H. Chan, L.-Y. Y. Ting, P.-Y. Y. Chen, C.-H. H. Liao, M.-L. L. Tsai, and H.-H. H. Chou, *ACS Catal.* **8**, 7766 (2018).
- [17] K. Lin, Z. Wang, Z. Hu, P. Luo, X. Yang, X. Zhang, M. Rafiq, F. Huang, and Y. Cao, *J. Mater. Chem. A* 19087 (2019).
- [18] J. Yu, X. Sun, X. Xu, C. Zhang, and X. He, *Appl. Catal. B Environ.* **257**, 117935 (2019).
- [19] R. S. Sprick, J.-X. Jiang, B. Bonillo, S. Ren, T. Ratvijitvech, P. Guiglion, M. A. Zwijnenburg, D. J. Adams, and A. I. Cooper, *J. Am. Chem. Soc.* **137**, 3265 (2015).

- [20] L. Li, W. Y. Lo, Z. Cai, N. Zhang, and L. Yu, *Macromolecules* **49**, 6903 (2016).
- [21] L. Li, Z. Cai, Q. Wu, W. Y. Lo, N. Zhang, L. X. Chen, and L. Yu, *J. Am. Chem. Soc.* **138**, 7681 (2016).
- [22] S. Bi, Z. Lan, S. Paasch, W. Zhang, Y. He, C. Zhang, F. Liu, D. Wu, X. Zhuang, E. Brunner, X. Wang, and F. Zhang, *Adv. Funct. Mater.* **27**, (2017).
- [23] Y. S. Kochergin, D. Schwarz, A. Acharjya, A. Ichangi, R. Kulkarni, P. Eliášová, J. Vacek, J. Schmidt, A. Thomas, and M. J. Bojdys, *Angew. Chemie Int. Ed.* **57**, 14188 (2018).
- [24] C. Yang, B. C. Ma, L. Zhang, S. Lin, S. Ghasimi, K. Landfester, K. A. I. Zhang, and X. Wang, *Angew. Chemie - Int. Ed.* **55**, 9202 (2016).
- [25] C. B. Meier, R. S. Sprick, A. Monti, P. Guiglion, J.-S. M. Lee, M. A. Zwijnenburg, and A. I. Cooper, *Polymer (Guildf)*. **126**, 283 (2017).
- [26] C. B. Meier, R. Clowes, E. Berardo, K. E. Jelfs, M. A. Zwijnenburg, R. S. Sprick, and A. I. Cooper, *Chem. Mater.* **31**, 8830 (2019).
- [27] J. Xie, S. A. Shevlin, Q. Ruan, S. J. A. Moniz, Y. Liu, X. Liu, Y. Li, C. C. Lau, Z. X. Guo, and J. Tang, *Energy Environ. Sci.* **11**, 1617 (2018).
- [28] Z.-A. A. Lan, Y. Fang, Y. Zhang, and X. Wang, *Angew. Chemie - Int. Ed.* **57**, 470 (2018).
- [29] X. Wang, L. Chen, S. Y. Chong, M. A. Little, Y. Wu, W.-H. Zhu, R. Clowes, Y. Yan, M. A. Zwijnenburg, R. S. Sprick, and A. I. Cooper, *Nat. Chem.* (2018).
- [30] T. Banerjee, F. Haase, G. Savasci, K. Gottschling, C. Ochsenfeld, and B. V. Lotsch, *J. Am. Chem. Soc. jacs*. 7b07489 (2017).
- [31] V. S. Vyas, F. Haase, L. Stegbauer, G. Savasci, F. Podjaski, C. Ochsenfeld, and B. V. Lotsch, *Nat. Commun.* **6**, 8508 (2015).
- [32] P. Pachfule, A. Acharjya, J. Roeser, T. Langenhahn, M. Schwarze, R. Schomäcker, A. Thomas, and J. Schmidt, *J. Am. Chem. Soc.* **140**, 1423 (2018).
- [33] E. Jin, Z. Lan, Q. Jiang, K. Geng, G. Li, X. Wang, and D. Jiang, *Chem* **5**, 1632 (2019).
- [34] R. S. Sprick, Y. Bai, A. A. Y. Guilbert, M. Zbiri, C. M. Aitchison, L. Wilbraham, Y. Yan, D. J. Woods, M. A. Zwijnenburg, and A. I. Cooper, *Chem. Mater.* **31**, 305 (2019).
- [35] Y. Xu, N. Mao, S. Feng, C. Zhang, F. Wang, Y. Chen, J. Zeng, and J.-X. Jiang, *Macromol. Chem. Phys.* **218**, 1700049 (2017).
- [36] M. Sachs, R. S. Sprick, D. Pearce, S. A. J. Hillman, A. Monti, A. A. Y. Guilbert, N. J. Brownbill, S. Dimitrov, X. Shi, F. Blanc, M. A. Zwijnenburg, J. Nelson, J. R. Durrant, and A. I. Cooper, *Nat. Commun.* **9**, (2018).
- [37] D. J. Woods, S. Hillman, D. Pearce, L. Wilbraham, L. Flagg, W. Duffy, I. McCulloch, J. Durrant, A. Guilbert, M. Zwijnenburg, R. S. Sprick, J. Nelson, and A. Cooper, *Energy Environ. Sci.* (2020).
- [38] M. Wagemaker, G. J. Kearley, A. A. van Well, H. Mutka, and F. M. Mulder, *J. Am. Chem. Soc.* **125**, 840 (2003).
- [39] N. Rosenbach, H. Jobic, A. Ghoufi, F. Salles, G. Maurin, S. Bourrelly, P. L. Llewellyn, T. Devic, C. Serre, and G. Férey, *Angew. Chemie Int. Ed.* **47**, 6611 (2008).
- [40] T. Pham, K. A. Forrest, M. Mostrom, J. R. Hunt, H. Furukawa, J. Eckert, and B. Space, *Phys. Chem. Chem. Phys.* **19**, 13075 (2017).

- [41] S. V. Ruffle, I. Michalarias, J.-C. Li, and R. C. Ford, *J. Am. Chem. Soc.* **124**, 565 (2002).
- [42] M. Liu, L. Chen, S. Lewis, S. Y. Chong, M. A. Little, T. Hasell, I. M. Aldous, C. M. Brown, M. W. Smith, C. A. Morrison, L. J. Hardwick, and A. I. Cooper, *Nat. Commun.* **7**, 12750 (2016).
- [43] A generalized density of states (GDOS) is the phonon spectrum measured from inelastic neutron scattering (INS). In contrast to the vibrational density of states, the GDOS involves a weighting of the scatterers (atoms) with their scattering powers σ/M (σ : cross section, M : mass). These are presently for various atoms in the units of [barns \cdot amu $^{-1}$]: H, 81.37; D, 3.8; C, 0.46; and N, 0.822.
- [44] R. T. Cygan, L. L. Daemen, A. G. Ilgen, J. L. Krumhansl, and T. M. Nenoff, *J. Phys. Chem. C* **119**, 28005 (2015).
- [45] K. Gong, Y. Cheng, L. L. Daemen, and C. E. White, *Phys. Chem. Chem. Phys.* **21**, 10277 (2019).
- [46] J. Teixeira, M.-C. Bellissent-Funel, S. H. Chen, and A. J. Dianoux, *Phys. Rev. A* **31**, 1913 (1985).
- [47] V. F. Sears, *Can. J. Phys.* **44**, 1279 (1966).
- [48] V. F. Sears, *Can. J. Phys.* **44**, 1299 (1966).
- [49] M. Bee, *Quasielastic Neutron Scattering* (Adam Hilger, United Kingdom, 1988).
- [50] K. Sköld and D. L. Price, *Neutron Scattering* (Academic Press, 1986).
- [51] A. Sjolander, *Ark. Fys.* **14**, (1958).
- [52] L. G. Squires, *Introduction to the Theory of Thermal Neutron Scattering* (Dover Publications, 1996).